Multi-Spectrum Method for the Determination of the Spectral Responsivity and the Short-Circuit Current of Photovoltaic Devices

David Hinken,* Carsten Schinke, Karsten Bothe, and Rolf Brendel

Herein, a method for the determination of the spectral responsivity (SR) and the short-circuit current under standard test conditions of photovoltaic devices (e.g., solar cells) is presented. This multi-spectrum SR method requires a spectrally tunable broadband light source irradiating the photovoltaic device with a large number of different spectra. For each spectrum, the light response of the device and the spectral irradiance in the measuring plane are measured. The spectral irradiances are integrated within predefined wavelength intervals and are incorporated together with the measured light response into an equation system which relates them to the (unknown) SR of the photovoltaic device. By solving the equation system, mathematically using regression algorithms, the SR is determined. Due to the usage of a broadband light source, the device operates at realistic injection conditions during measurements. The mathematical background of the multi-spectrum SR method is described and its applicability is demonstrated on three world-photovoltaic-scale-type solar cells and one large-area reference cell. Short-circuit currents from all SR curves are calculated using the tabulated AM1.5 G spectrum. In comparison to the SR reference data, the short-circuit currents from the multi-spectrum SR method deviate by less than 0.68%.

1. Introduction

The spectral responsivity (SR) is a measure of the short-circuit current contribution generated by the respective spectral irradiance. Measured as a function of wavelength, the resulting SR curves are used in three essential applications: a) they allow for the calculation of the short-circuit current of a photovoltaic device for a given spectral irradiance, b) they provide insights into recombination and optical properties in the different layers of photovoltaic devices,[1–6] and c) they are required to calculate

the spectral mismatch correction factor[7] which is essential for an accurate determination of the short-circuit current of the photovoltaic device under standard test conditions (STC)[7] when using a reference device.

The measurement of SR curves for photovoltaic devices has been demonstrated using different measurement techniques. From a historic point of view, as described in the overview from Hartman et al.[8] in 1982, first facilities used a broadband light source together with bandpass filters or grating-based monochromators to generate monochromatic light irradiating the solar cell. The monochromatic light can hereby either be used directly, allowing for a direct determination of the current response using a multimeter, or it can be chopped and superimposed on an additional time–constant bias light source. For this dual-beam technique, the resulting current response is analyzed with a lock-in amplifier system filtering out the pulsing current generated from the monochromatic light. In both cases, the resulting current response from the solar cell under test is compared to the current response from a reference device with known SR and the SR of the solar cell under test directly follows. In contrast to the direct usage of the monochromatic light, the dual-beam technique allows to measure nonlinear solar cells (short-circuit current is not linear to the irradiance). However, it increases the complexity of the measurement facility because lock-in technique is required. In 1986, application of the dual-beam technique to solar cell areas up to 4 cm² was shown by Boivin et al.,[9] dealing with bias currents up to 50 mA. Shortly after, in 1987, Metzdorf[10] introduced the differential SR (DSR) method which is an extension of the dual-beam technique requiring not only one measurement at one specific bias light intensity but various measurements at different bias light intensities. Thereby, a physically correct calculation of the SR and the short-circuit current of the photovoltaic device becomes possible even for highly nonlinear cells. This DSR method is used in the IEC60904:08 standard[11] as reference method for the determination of SR curves and is widely used for primary reference cell calibration at national metrology institutes (NMI)[12] and for solar cell calibration at calibration laboratories.[13,14] Today's measurement facilities have demonstrated

D. Hinken, K. Bothe, R. Brendel
Institute for Solar Energy Research in Hamelin
31860 Emmerthal, Germany
E-mail: hinken@isfh.de

C. Schinke, R. Brendel
Institute for Solid State Physics
Leibniz Universität Hannover
30167 Hannover, Germany

The ORCID identification number(s) for the author(s) of this article can be found under https://doi.org/10.1002/solr.202300240.

usage of DSR measurement technique on solar cells with areas up to 275 cm², dealing with bias currents up to 12 A.[14]

While measurement results with very low measurement uncertainties have been reported[15] for the DSR method, its application requires complex lock-in technique and measurements at different bias light intensities with irradiances up to 1000 W m⁻² (or slightly above). This becomes especially challenging for very large-area solar cells (nowadays with cell areas up to 441 cm², wafer format M12) because the current generated by the bias light scales in first-order linearly with the area of the solar cell while the pulsed current of the monochromatic light remains constant. To overcome this limitation, measurement facilities with wavelength-tunable lasers were developed[16,17] increasing the intensity of the monochromatic light but also the complexity of the measurement system itself. Another possibility to decouple from the growing bias current was developed by Fischer et al.[6] who used a lateral scanning system which irradiates only a small region of the solar cell at the same time. This approach allows scalability to large-area solar cells but requires an x–y scan of the solar cell and such total measurement time increases. Other options to face the growing bias current are simplifications given in the IEC60904:08 standard[11,18] allowing to measure at 300 or even 100 W m⁻² bias light if the solar cell is linear. Alternatively, light-emitting diodes (LEDs) may be used for the generation of monochromatic light. LEDs are solid-state devices and are available in high-power versions. In principle, they allow for a direct quasi-monochromatic light generation over a large wavelength range without requiring additional filters. First description of the usage of LEDs for SR measurements dates back to 1996. Tulloch[19] used five LEDs with different wavelengths to determine the SR of photodetectors. This method was further exploited by Young et al. in 2008[20] using a parallel modulation of all available LEDs with different frequencies together with an advanced digital signal processing, which allowed for very fast measurements. In 2013, Hamadani et al.[21] discussed different modulation techniques and bias light applications for such an LED-based SR measurement facility. While correction procedures for the broad emission spectrum of LEDs have been proposed,[22–24] the main challenge is the limited wavelength resolution of the SR curve in general, because each supporting point requires an appropriate LED.

In this article, we introduce a method which utilizes a tunable broadband light source to determine the SR curve and the short-circuit current of a photovoltaic test device under STCs. For this multi-spectrum SR method, the photovoltaic device is irradiated with multiple broadband spectra that all differ from each other. For each spectrum, the current response (i.e., the short-circuit current) of the photovoltaic device is measured. We utilize the relation between the incident spectral irradiance and the measured current response resulting in an equation system which is solved mathematically and yields as solution the SR curve of the photovoltaic device.

Our novel multi-spectrum SR method has various advantages compared to the traditional approaches. It is a fully steady-state technique, no dual-beam irradiation or modulation of the irradiating spectrum is required. This reduces complexity of the measurement equipment since no lock-in technique is required. Moreover the SR related to standard test conditions, and consequently the short-circuit current of the cell, can directly be determined without the need of measurements at various bias irradiances. In addition to short-circuit conditions, also other operating points (e.g., the maximum power point voltage) can directly be utilized, allowing for a more accurate analysis of non-linear devices.

For the multi-spectrum SR method, broadband spectra are required. In case an LED-based sun simulator is used, spectral broadening or broadband LEDs are no limitation for the applicability of the method as long as sufficient variation along the spectrum can be guaranteed. A further difference to all previous SR measurement techniques is that the multi-spectrum SR method does not require a primary calibrated reference solar cell. Instead, a (calibrated) spectroradiometer is used as primary standard. The multi-spectrum SR method is fast and can directly be integrated into a current–voltage (I–V) measurement facility based on an LED sun simulator. Thus, no extra equipment is required except for the spectroradiometer.

2. Theory

The SR of a photovoltaic device under STC[25] is the ratio of short-circuit current contribution $I_{\lambda,\mathrm{STC}}(\lambda)$ (mA nm⁻¹) to spectral irradiance $E_{\lambda,\mathrm{AMx}}(\lambda)$ (W m⁻² nm⁻¹)

$$s_{\mathrm{STC}}(\lambda) = \frac{I_{\lambda,\mathrm{STC}}(\lambda)}{E_{\lambda,\mathrm{AMx}}(\lambda)} \qquad (1)$$

while the device is irradiated with the spectrum AMx. AMx is usually replaced by the AM1.5 G spectrum[7] but other spectra are possible, too. Note that the SR can be defined analogously also for other operating points. By definition, the integration of $I_{\lambda,\mathrm{STC}}(\lambda)$ over all wavelengths gives the short-circuit current

$$I_{\mathrm{STC}} = \int d\lambda I_{\lambda,\mathrm{STC}}(\lambda) \qquad (2)$$

of the device under STC. Inserting Equation (1) in (2) directly gives

$$I_{\mathrm{STC}} = \int d\lambda E_{\lambda,\mathrm{AMx}}(\lambda) s_{\mathrm{STC}}(\lambda) \qquad (3)$$

which relates the incident spectral irradiance and the SR with the extracted current. For a spectrum $E_\lambda(\lambda)$, only slightly differing from $E_{\lambda,\mathrm{AMx}}(\lambda)$, the latter equation can be written as

$$I_{\mathrm{meas}} = \int d\lambda E_\lambda(\lambda) s_{\mathrm{STC}}(\lambda) \qquad (4)$$

where I_{meas} gives the measured current when the photovoltaic device is irradiated with $E_\lambda(\lambda)$.

For the multi-spectrum SR method, the current and the spectral irradiance is measured N times, giving I_{meas}^n and $E_\lambda^n(\lambda)$ data sets, with $n = 1..N$. For each one of these N combinations, Equation (4) holds

$$I_{\mathrm{meas}}^n = \int d\lambda E_\lambda^n(\lambda) s_{\mathrm{STC}}(\lambda) \qquad (5)$$

giving a system of N equations. To solve this system, the integral is split in K wavelength intervals $[\lambda_{\text{left}.k}..\lambda_{\text{right}.k}]$, with $k = 1..K$ and $\lambda_{\text{right}.k} = \lambda_{\text{left}.k+1}$, and written as a sum

$$
\begin{aligned}
I_{\text{meas}}^n = &\int_{\lambda_{\text{left}.1}}^{\lambda_{\text{right}.1}} d\lambda E_\lambda^n(\lambda) s_{\text{STC}}(\lambda) \\
&+ \int_{\lambda_{\text{left}.2}}^{\lambda_{\text{right}.2}} d\lambda E_\lambda^n(\lambda) s_{\text{STC}}(\lambda) \\
&+ \cdots \\
&+ \int_{\lambda_{\text{left}.K}}^{\lambda_{\text{right}.K}} d\lambda E_\lambda^n(\lambda) s_{\text{STC}}(\lambda)
\end{aligned}
\tag{6}
$$

As approximation, we assume the SR to be constant within each wavelength interval, for example, $s_{\text{STC},1}$ approximates $s_{\text{STC}}(\lambda)$ in the wavelength interval from $\lambda_{\text{left}.1}$ to $\lambda_{\text{right}.1}$. Naturally, this approximation is more accurate if the wavelength intervals are small or if the SR is varying little with respect to wavelength within the wavelength interval. Using this approximation, Equation (6) can be simplified to

$$
I_{\text{meas}}^n \approx s_{\text{STC},1} P_1^n + s_{\text{STC},2} P_2^n + \cdots + s_{\text{STC},K} P_K^n
\tag{7}
$$

where each irradiance P_k^n (with $k = 1..K$) is given by

$$
P_k^n = \int_{\lambda_{\text{left}.k}}^{\lambda_{\text{right}.k}} d\lambda E_\lambda^n(\lambda)
\tag{8}
$$

Equation (7) gives a system of N equations and K unknowns ($s_{\text{STC},1}$ to $s_{\text{STC},K}$)

$$
\begin{pmatrix} I_{\text{meas}}^1 \\ I_{\text{meas}}^2 \\ \vdots \\ I_{\text{meas}}^N \end{pmatrix} \approx \begin{pmatrix} P_1^1 & P_2^1 & \cdots & P_K^1 \\ P_1^2 & P_2^2 & \cdots & P_K^2 \\ \vdots & \cdots & \ddots & \vdots \\ P_1^N & P_2^N & \cdots & P_K^N \end{pmatrix} \cdot \begin{pmatrix} s_{\text{STC},1} \\ s_{\text{STC},2} \\ \vdots \\ s_{\text{STC},K} \end{pmatrix}.
\tag{9}
$$

The latter equation system can be solved by known mathematical numerical procedures[26] (e.g., least-square regression) or analytically using inverse matrices[27] if the system is exactly determined (i.e., the matrix is of quadratic shape, $N = K$). As a result, the values $s_{\text{STC},k}$ are obtained. For plotting and postprocessing, a wavelength λ_k, with $\lambda_{\text{left}.k} \leq \lambda_k \leq \lambda_{\text{right}.k+1}$ has to be assigned to each $s_{\text{STC},k}$ value. While the mid-wavelength

$$
\lambda_k = \frac{\lambda_{\text{left}.k} + \lambda_{\text{right}.k}}{2}
\tag{10}
$$

is a natural choice for equidistant wavelength intervals the best choice of λ_k might differ for non-equidistant wavelength intervals (see e.g., Section 4).

Finally, the resulting curve $s_{\text{STC},k}(\lambda_k)$ is obtained representing the $s_{\text{STC}}(\lambda)$ curve of the photovoltaic device under test. In addition, using Equation (3), also the short-circuit current under STC, I_{STC}, directly follows.

3. Measurement Facility

We demonstrate the multi-spectrum SR method using a custom-build $I-V$ measurement system used for solar cell calibration of M10 and M12 solar cells. A picture and a sketch of this system is shown in **Figure 1**a,b. It comprises an LED sun simulator
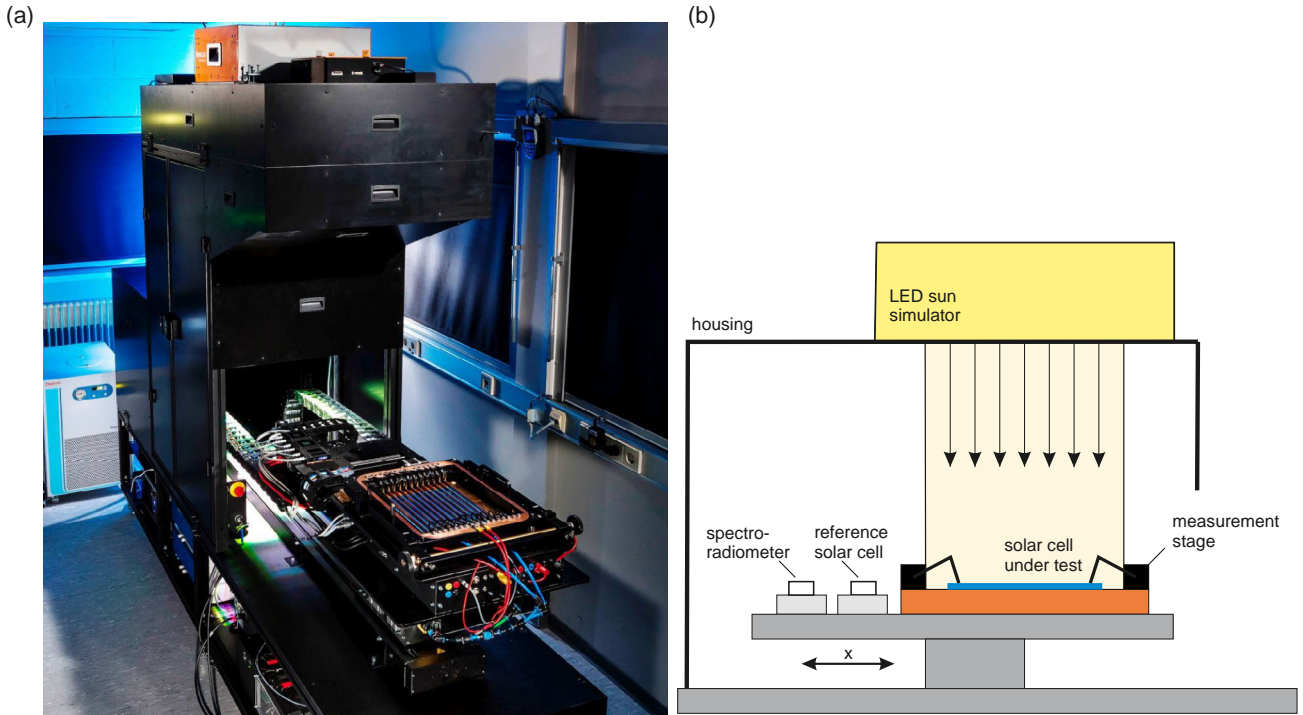

Figure 1. a) Photograph and b) sketch of the I–V measurement facility at ISFH CalTeC with LED-based sun simulator which is used to demonstrate the multi-spectrum SR method.

(Wavelabs SINUS-360 Plus), a spectroradiometer (Instrument Systems CAS 140 CT), a temperature-controlled contacting stage for different cell types (custom build), and electrical equipment to measure the I–V characteristics of the photovoltaic device (multimeter and I–V source). The spectroradiometer is calibrated at the Calibration and Test Center (CalTeC) of the Institute for Solar Energy Research Hamelin (ISFH) using a quartz–tungsten halogen lamp as reference,[28] whose spectral irradiance is calibrated at Germany's national metrology laboratory, the Physikalisch–Technische Bundesanstalt (PTB). The resistance for current measurement and also the multimeters are calibrated at accredited laboratories. The spectroradiometer and the contacting stage are built onto a motorized axis which allows for rapid switching between the spectroradiometer and the photovoltaic device under test.

The LED sun simulator has 27 LED channels of different wavelengths, covering a wavelength range from 346.1 to 1194.8 nm (peak wavelengths of first/last LED channel). In its standard configuration, the spectrum of the sun simulator classifies[29] as A++ and its inhomogeneity of the light field in the measuring plane as A+. Photovoltaic devices with an area of up to $220 \, mm \times 220 \, mm$ can be irradiated. The irradiance is stabilized using a silicon monitor diode. The sun simulator allows to set custom intensities for the LED channels to set a specific target spectrum. **Figure 2**a shows the normalized spectra of all 27 LED channels and Figure 2b shows the AM1.5 G base spectrum of the sun simulator (green solid line) together with the tabulated AM1.5 G spectrum (black solid line). In addition, this figure exemplarily shows one of the modified spectra (red solid line)
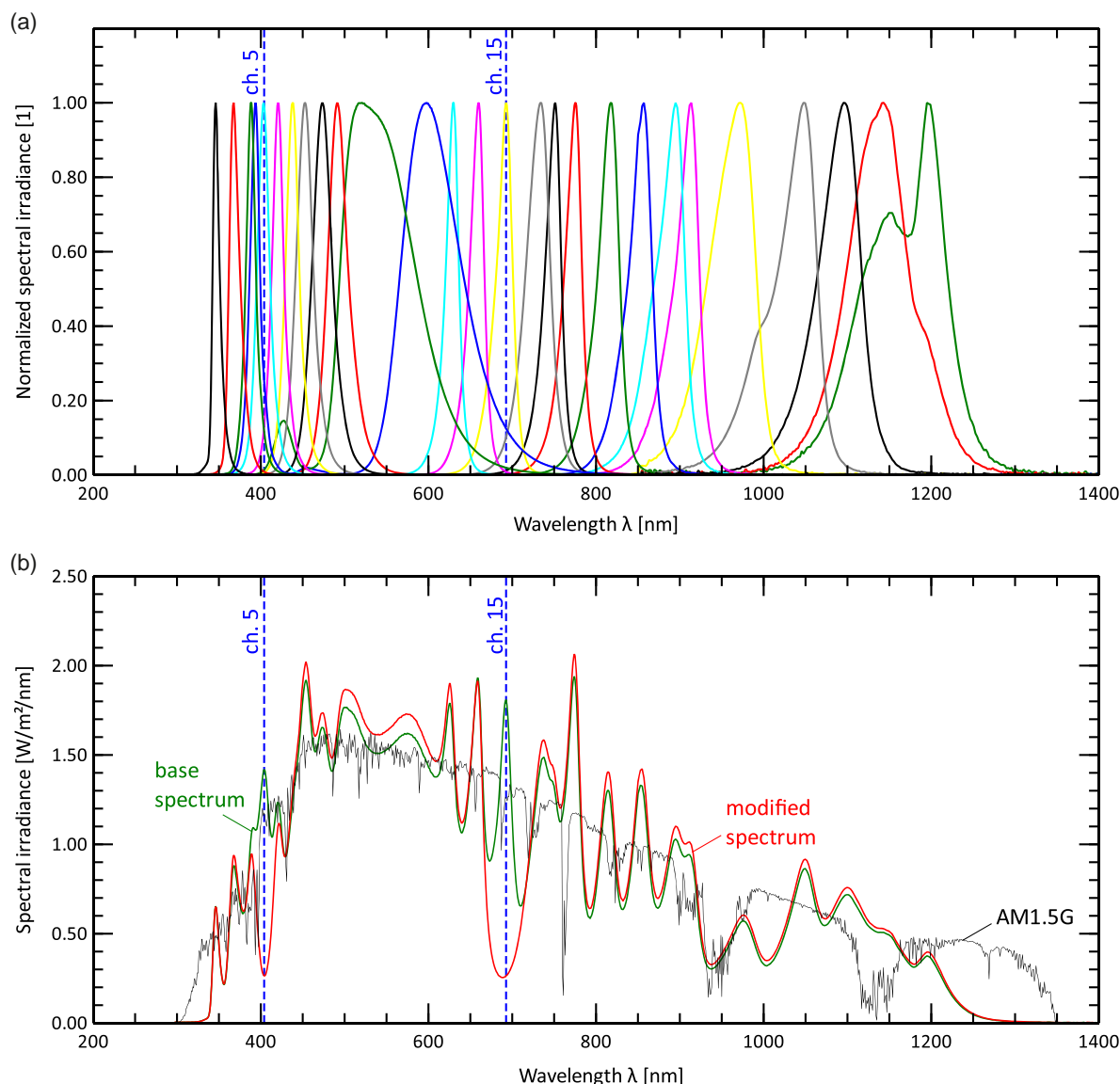

Figure 2. a) Spectra of all 27 channels of the sun simulator, normalized to its maximum spectral irradiance. b) Base spectrum of the sun simulator (green solid line) together with the tabulated AM1.5 G spectrum (black solid line) and a modification of the base spectrum (red solid line). The modified spectrum is an adaption from the base spectrum and changes the intensity setting of channel $C_X = 5$ and channel $C_Y = 15$ (marked with blue dashed lines) to zero.

as it is used by the multi-spectrum SR method. The modified spectrum has less intensity on channels 5 and 15. For all other channels, a slight increase in intensity is noticeable. This is a result of the irradiance stabilization with the monitor diode: the stabilization compensates the reduced intensity of channels 5 and 15 by slightly increasing the intensity of all LED channels. Note that this is not a requirement for the multi-spectrum SR method which also works if all other channels maintain their intensities.

For the implementation of the multi-spectrum SR method, the photovoltaic device under test has to be irradiated with N different spectra. All these spectra use the base spectrum and introduce modifications. For a first demonstration, we choose a two-channel modification. For each spectrum, the intensity of channels

$$C_X \in 1, 2, \ldots, 27 \tag{11}$$

and

$$C_Y = \begin{cases} C_X + 10 & \text{for } C_X <= 17 \\ C_X + 10 - 27 & \text{for } C_X > 17 \end{cases} \tag{12}$$

is modified by a factor X for channel C_X and Y for channel C_Y, resulting in $N_{XY} = 27$ spectra and currents. The example given in **Figure 3**b, shown as red solid line, is the base spectrum modified in channel $C_X = 5$ and channel $C_Y = 15$ using channel intensity multiplication factors $X = 0.0$ and $Y = 0.0$ (denoted in the following with 0.0–0.0). In total, we choose four combinations for X and Y, 0.0–0.0, 0.0–1.0, 2.0–0.0, and 2.0–1.0, giving a total of $N = 4 \times 27 = 108$ spectra. Note that this spectra generation has not been further optimized. Probably, better spectral choices are possible, such further increasing the quality of the results or reducing the time of data acquisition.

The measurements for each XY combination are carried out in two steps: first, the spectroradiometer is placed in the measuring plane to measure all N_{XY} spectra. Second, the photovoltaic device is moved into the measurement plane. After temperature stabilization to 25.0 °C, all N_{XY} currents are measured. This sequence is repeated with each one of the four XY combinations. Currently, in our measurement system, one N_{XY} measurement requires about 4 min, total measurement time for four combinations is 16 min.

For the analysis of the acquired measurement data (N spectra and currents), the wavelength range has to be split from $\lambda_{\text{left.1}}$ to $\lambda_{\text{right.}K}$ in K wavelength ranges. As the LED light source consists of $M = 27$ wavelength distributions (compare with Figure 2), we choose $K = M$ and measure all peak wavelengths $\lambda_{\text{peak.}k}$. For $2 \leq k \leq K - 1$, we define the wavelength intervals being at

$$\lambda_{\text{left.}k} = \lambda_{\text{peak.}k} - \frac{\lambda_{\text{peak.}k} - \lambda_{\text{peak.}k-1}}{2} \tag{13}$$

$$\lambda_{\text{right.}k} = \lambda_{\text{peak.}k} + \frac{\lambda_{\text{peak.}k+1} - \lambda_{\text{peak.}k}}{2} \tag{14}$$

For $k = 1$, we set

$$\lambda_{\text{left.1}} = \lambda_{\text{peak.1}} - 5 \text{ nm} \tag{15}$$

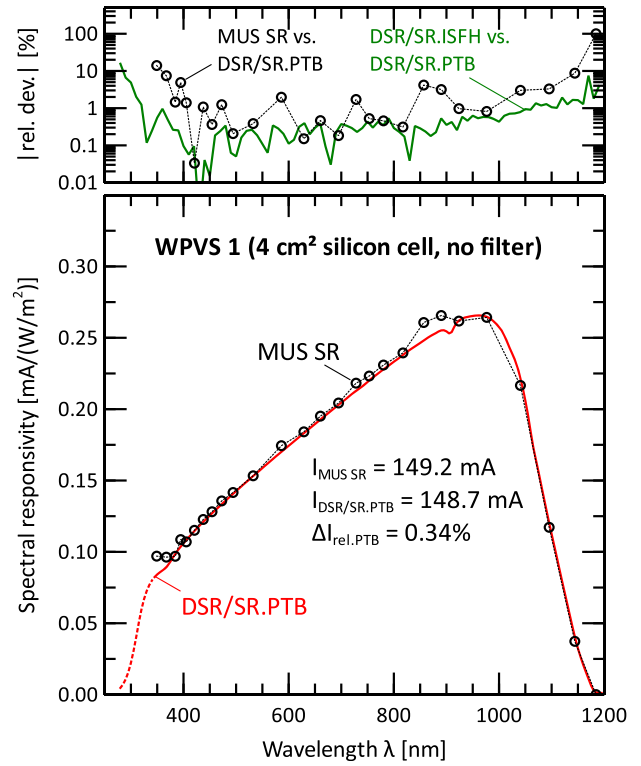$$\lambda_{\text{right.1}} = \lambda_{\text{left.2}} \tag{16}$$

Figure 3. Black open circles: application of the multi-spectrum SR method (abbreviated as MUS SR) to an unfiltered world-photovoltaic-scale (WPVS) solar cell. Red solid line: standard differential spectral responsivity (DSR)/SR procedure for comparison. The AM1.5 G short-circuit currents I_{MUSSR} (calculated with the multi-spectrum SR data) and $I_{\text{DSR/SR}}$ (calculated with the DSR/SR data) are given together with the relative deviation between both values. Top graph: relative deviations of the multi-spectrum SR method to the DSR/SR Physikalisch–Technische Bundesanstalt (PTB) data and benchmark data comparing DSR/SR from ISFH CalTeC and PTB.

Similarly, for $k = K$, we set

$$\lambda_{\text{left.}K} = \lambda_{\text{right.}K-1} \tag{17}$$

$$\lambda_{\text{right.}K} = \lambda_{\text{peak.}K} + 5 \text{ nm} \tag{18}$$

As wavelength λ_k, we choose the peak-wavelength itself

$$\lambda_k = \lambda_{\text{peak.}k} \tag{19}$$

Using these wavelength ranges, the irradiances P_k^n can be calculated from the measured spectra using Equation (8). Together with the measured currents I_{meas}^n, the required equation system with N equations and K unknowns is obtained and solved. The data analysis is implemented with the Python programming language.[30] For solving the equation system, we use the numerical least-square solver *lsq_linear* from the package *scipy.optimize*.[31] As constraint for the least-square regression, we choose a lower bound of zero for all $s_{\text{STC,k}}$ values.

**ADVANCED
SCIENCE NEWS**

www.advancedsciencenews.com

Solar
RRL

www.solar-rrl.com

4. Experimental Demonstration

For the demonstration of the multi-spectrum SR method, we select various solar cells. At least one cell shall cover the full wavelength range of silicon, one cell shall cover a wavelength range similar to perovskite or gallium arsenide cells, and one device shall cover the long-wavelength range (e.g. 700 to 1200 nm). In addition, the demonstration shall cover typical solar cell areas. Also, the test solar cells shall provide simple contacting that does not induce additional shading.

Three of the four selected solar cells are world-photovoltaic-scale (WPVS)-type silicon solar cells[32] with an active surface area of $\approx 4.0\,cm^2$. While WPVS 1 incorporates a standard cover glass, WPVS 2 and WPVS 3 comprise an additional filter to make the device wavelength selective. The fourth device is a WPVS-like large-area reference solar cell (commercially available from Ingenieurbüro Mencke & Tegtmeyer GmbH[33]) with an active surface area of 245.7 cm^2 (wafer size M2). Here, WPVS-like means that the original WPVS design[32] of the cell package was modified to use a large-area solar cell.

The multi-spectrum SR method is applied to all four devices and the resulting SR values are shown in **Figure** 3, **4**, **5** and **6** as black open circles. In addition, comparison data from the standard DSR/SR procedure is shown as red solid line. This data stems either from Germany's NMI, the PTB, or from ISFH's solar cell calibration laboratory, the ISFH CalTeC. For all devices, the AM1.5 G short-circuit current I_{MUSSR} (calculated with the multi-spectrum (MUS) SR data) and $I_{DSR/SR}$ (calculated with the DSR/SR data) are given within the graphs together with the relative deviation

$$\Delta I_{rel.a} = \frac{I_{MUSSR}}{I_{DSR/SR.a}} - 1 \tag{20}$$

with a = PTB when comparing MUS SR with PTB data (Figure 3–5) and a = ISFH (Figure 6) when comparing with ISFH CalTeC data. Note that for the current calculation from the DSR/SR data, only the wavelength region from the MUS SR method was considered (ranging from $\lambda_{left.1}$ to $\lambda_{right.K}$). Hence, the data shown as dashed red line in the figures is not used for the calculation of the short-circuit current. To allow for a quantitative analysis, an additional graph showing the relative deviations between the values obtained from the MUS SR and the reference DSR/SR method is shown on top of each SR graph (black open circles)

$$\Delta s_{rel.1.a} = \left| \frac{s_{MUSSR}(\lambda)}{s_{DSR/SR.a}(\lambda)} - 1 \right| \tag{21}$$

Again a = PTB (Figure 3–6, denoted with MUS SR vs. DSR/SR.PTB) and a = ISFH (Figure 6, denoted with MUS SR vs. DSR/SR.ISFH) are used. To have a benchmark for the obtained relative deviations between the MUS SR and the DSR/SR data from PTB, we add the relative deviation of the SR obtained by the DSR/SR measurement facility at ISFH CalTeC compared to PTB data (green solid line in top graph, denoted with DSR/SR.ISFH vs. DSR/SR.PTB)
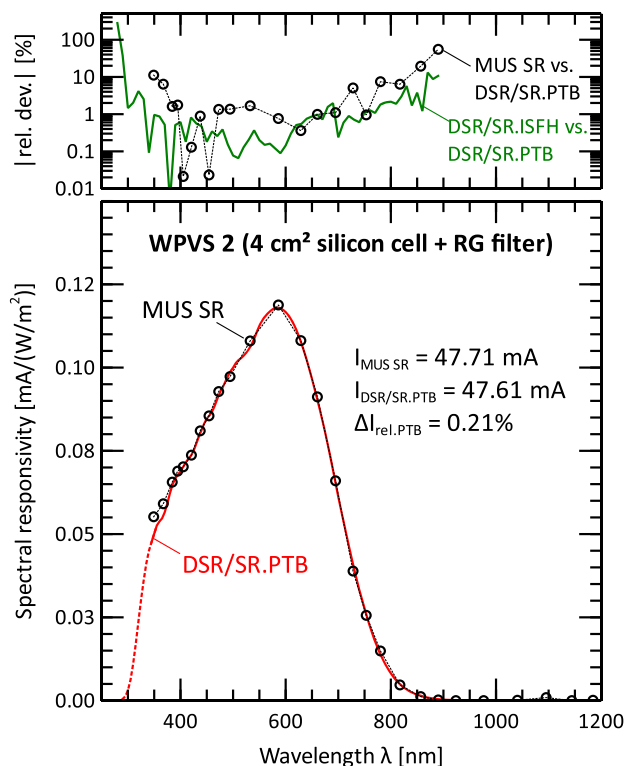

Figure 4. See Figure 3 for description of the figure. Here, the solar cell is a short-pass filtered WPVS solar cell.
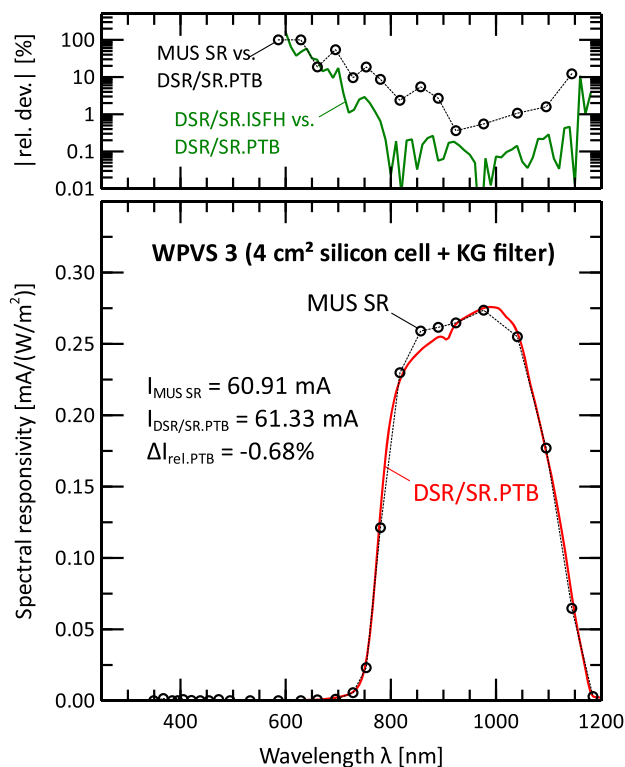

Figure 5. See Figure 3 for description of the figure. Here, the solar cells is a long-pass filtered WPVS solar cell.
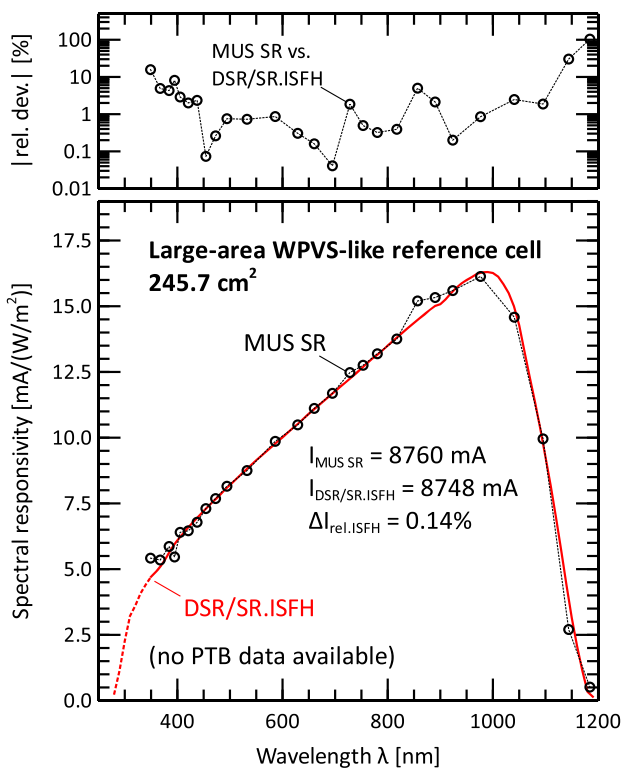
Figure 6. See Figure 3 for description of the figure. Here, the solar cells is a large-area WPVS-like reference cell.

$$\Delta s_{\mathrm{rel.2.PTB}}(\lambda) = \left| \frac{s_{\mathrm{DSR/SR.ISFH}}(\lambda)}{s_{\mathrm{DSR/SR.PTB}}(\lambda)} - 1 \right| \qquad (22)$$

This comparison is possible for Figures 3–5 but not for Figure 6 because no PTB data is available.

Figure 3 shows the result of the multi-spectrum SR method for WPVS 1, the unfiltered silicon WPVS solar cell. The figure shows that the multi-spectrum SR and the DSR/SR reference data (PTB data) have a very similar shape and that the vast majority of the determined SR values of the multi-spectrum SR method match the reference data. A calculation of the short-circuit current under STC conditions gives 149.2 mA for the multi-spectrum SR method. It overestimates the value from the DSR/SR method (148.7 mA) by 0.34%. As shown in the top graph, relative deviations of the spectral responsivities are smaller than 14% over the whole wavelength range up to 1170 nm. The largest relative deviations are present in the very short-wavelength range and in the very long wavelength range where the SR already is very small and thus relative deviations are not very meaningful any more. Comparing these relative deviations to the benchmark data (DSR/SR data from ISFH CalTeC compared to the PTB data, green line in top chart) reveals that some wavelength regions are present where the relative deviations are comparable. However, in general, the relative deviation of the multi-spectrum SR method is half an order of magnitude larger than the benchmark data.

Figure 4 shows the result for WPVS 2, the short-pass filtered silicon solar cell. Also, here a good consistency between the

multi-spectrum SR and DSR/SR method can be observed. The shape of the SR-curve is well reproduced. Even the small modulations in SR in the wavelength range from 350 to 570 nm, probably a result from the short-pass filter, appear in the multi-spectrum SR curve. In terms of short-circuit current I_{STC}, WPVS 2 shows an excellent agreement of 0.21%. For this cell, the relative deviations (as shown in the top graph) are again about half an order of magnitude higher than that of the benchmark data.

Figure 5 shows the results for WPVS 3, the long-pass filtered silicon solar cell. Again, we observe a good consistency between the multi-spectrum SR and DSR/SR method. The shape of the whole SR curve is well reproduced. Even the steep increase of SR at ≈790 nm as well as the values in the wavelength range with no current collection (up to ≈700 nm) is accurately reproduced. The short-circuit currents are 60.91 mA (multi-spectrum SR method) and 61.33 mA (PTB data). Hence, the multi-spectrum SR method underestimates the short-circuit current by −0.68%. The relative deviations as shown in the top graph, compared to the benchmark data, are about one order of magnitude higher. It has to be noted that the used light source provides more LED channels in the wavelength-region of device WPVS 1 and 2 than for WPVS 3 (compare with Figure 2). Hence, the resulting wavelength resolution is higher for WPVS 1 and 2 than for WPVS 3.

Figure 6 shows the results for a large-area WPVS-like reference cell. Reference data stems from ISFH CalTeC as no PTB data is available. Also for this large-area device the multi-spectrum SR and DSR/SR methods give consistent results. It demonstrates that the irradiation of the solar cell is sufficiently homogeneous and that also the currents, being nearly two magnitudes higher compared to the WPVS cells, are measured with sufficient precision. For this device, the resulting STC short-circuit current is 8760 mA (multi-spectrum SR method) which compares to 8748 mA (DSR/SR method) and deviates by 12 mA only (0.14%). Relative deviations (top graph of Figure 3) are within the same range as for the WPVS cell in Figure 4 indicating that the scaling to a large-area device does not negatively affect the accuracy of the results. The remaining deviations are thus probably limited by other effects.

5. Discussion and Outlook

The results of the multi-spectrum SR method are consistent to the traditional DSR/SR method. The shape of the SR-curve is well reproduced for all four devices. Even sharp increases of the SR (WPVS 3) and small modulations in the SR-curve (WPVS 2), that are probably caused by the filters on top of the cells, are reproduced by the multi-spectrum SR method.

The relative deviations shown in the top graphs of Figure 3–6 reveal two wavelength regions where systematic deviations are identified. An overestimation of the multi-spectrum SR method is visible in the short-wavelength region from 350 to 370 nm for devices WPVS 1, WPVS 2, and the large-area cell. It is not visible for WPVS 3 because the SR is negligibly small in this region for this device. Similarly, the wavelength region from 850 to 900 nm shows another overestimation present in the investigated devices (WPVS 1, WPVS 3, and the large-area cell). Possible explanations for these overestimations are intensity drifts of the LED

channels, lateral inhomogeneities or stray light within the spectroradiometer and have to be further investigated.

Regarding the short-circuit current, relative deviations of 0.34%, 0.21%, −0.68%, and 0.14% are obtained for the four devices. We compare these values to measurement uncertainties at ISFH CalTeC, which typically are around ±1.0% (level of confidence of approximately 95%[34]) for small and large-area devices[14] and to measurement uncertainties from NMI reaching values down to ±0.50%.[35] For WPVS 1, WPVS 2, and the large-area reference cell, the relative deviations obtained are smaller than these typical measurement uncertainties. WPVS 3 shows a larger relative deviation of −0.68%, probably caused from the lower wavelength resolution in this region. To judge on the consistency in terms of SR and short-circuit current between the multi-spectrum SR and the DSR/SR method, it has to be taken into account that absolute values were determined using different measurement techniques and completely different primary standards. While the DSR/SR methods utilizes a calibrated WPVS solar cell, the multi-spectrum SR method utilizes a spectroradiometer which is calibrated using a quartz-tungsten halogen lamp as reference.

Application of the multi-spectrum SR method to back-contacted bare solar cells is directly possible. Similarly, it can directly be applied on two-side-contacted solar cells if the front-side contacting is realized via contacting probes which do not induce a shadow on the cell. However, most two-side solar cells are contacted with bars from the front side which induce a shadow on the cell. Regarding the application of the multi-spectrum SR method with this type of contacting the shadowing can either be neglected, such as giving an SR curve (and I_{STC} value) reduced by the shadowing factor, or correction procedures similar to the ones available for the determination of the short-circuit current have to be applied.[14] Application of the multi-spectrum SR method is also possible on irradiance sensors and solar modules, enabling a quick possibility to determine SR-curves for these devices. Heating of the device might be prevented by irradiating the device only shortly with each spectrum. In case of an irradiance sensor with shunt resistor, which maintains the photovoltaic device near short-circuit conditions, the resulting voltage drop can be used as current response. In addition to LED lamp systems with tunable spectrum, also filter add-ons for xenon/halogen lamps can be used. While the transmission of these filters has to differ from each other, it is not required that they are, for example, specially designed bandpass filters.

In addition to short-circuit conditions, also maximum power point conditions can be utilized as operating point, which is important for a cell analysis of, for example, perovskite solar cells where the recombination properties depend on ionic accumulation within the cell itself.[36] The multi-spectrum SR method gives an additional benefit when it is applied to perovskite solar cells because it operates under steady-state light conditions and perovskite solar cells are known to show a frequency dependency during DSR measurements.[37]

For a full application of the multi-spectrum SR method, it is recommended to have also light (LEDs) available in the wavelength region from 300 to 340 nm. LEDs within this wavelength region are commercially available and it should be possible to directly integrate them within an LED sun simulator or as an add-on to provide these additional wavelengths. It has to be further analyzed how the base spectrum has to be modified to get best results and a higher wavelength resolution.

6. Conclusion

We introduced the multi-spectrum SR method to determine the SR of photovoltaic devices. This method requires a set of N different spectra which irradiate the photovoltaic device consecutively. For each spectrum, the resulting current response and the spectrum at the measuring plane are determined. Both quantities are then converted into a set of linear equations which can be solved analytically or numerically. The applicability of the multi-spectrum SR method was demonstrated on four encapsulated solar cells with active areas of 4.0 and 245.7 cm². Resulting spectral responsivities were consistent in comparison to reference data obtained from the DSR/SR method. By calculating the STC short-circuit currents, we demonstrated the overall accuracy of the new method. For the three WPVS devices, the relative deviation in I_{STC} was 0.34%, 0.21%, and −0.68%, and for the large-area WPVS-like reference cell, the relative deviation was 0.14%. In comparison to traditional DSR/SR methods, a reference cell, with calibrated DSR values, is not required. Instead, the multi-spectrum SR method utilizes a calibrated spectroradiometer. A benefit of the new method is that even for very large-area solar cells or modules, the device operates at standard injection conditions, which is especially important for nonlinear devices. Furthermore, no complex lock-in technique is required and also the data acquisition is more simple.

Conflict of Interest

The authors declare no conflict of interest.

Data Availability Statement

The data that support the findings of this study are available from the corresponding author upon reasonable request.

Keywords

[1] P. Basore, in *Conf. Record of the Twenty Third IEEE Photovoltaic Specialists Conf., – 1993 (Cat. No.93CH3283-9)*, IEEE, Piscataway, NJ **1993** pp. 147–152.

[2] J. Rand, P. Basore, in *The Conf. Record of the Twenty-Second IEEE Photovoltaic Specialists Conf. – 1991*, Vol. 1, IEEE, Piscataway, NJ **1991** pp. 192–197.

[3] J. M. Gee, in *Conf. Record of the Twenty Fifth IEEE Photovoltaic Specialists Conf.*, IEEE, Piscataway, NJ 1996, pp. 557–560.

[4] R. Brendel, M. Hirsch, R. Plieninger, J. Werner, *IEEE Trans. Electron Dev.* **1996**, *43*, 7.

[5] M. Spiegel, B. Fischer, S. Keller, E. Bucher, in *Conf. Record of the IEEE Photovoltaic Specialists Conf.*, IEEE, Piscataway, NJ **2000**, 2000-Janua 311.

[6] B. Fischer, Ph.D. Thesis, **2003**, http://en.scientificcommons.org/31058651.

[7] International Standard IEC 60904-03, Edition 4.0, 2019-02, Photovoltaic Devices – Part 3: Measurement Principles for Terrestrial Photovoltaic (PV) Solar Devices with Reference Spectral Irradiance Data.

[8] J. S. Hartman, M. A. Lind, *Sol. Cells* **1982**, *7*, 147.

[9] L. P. Boivin, W. Budde, C. X. Dodd, S. R. Das, *Appl. Optics* **1986**, *25*, 2715.

[10] J. Metzdorf, *Appl. Optics* **1987**, *26* 1701.

[11] International Standard IEC 60904-08, Edition 3.0, 2014-05, Photovoltaic Devices - Part 8: Measurement of Spectral Responsivity of a Photovoltaic (PV) Device.

[12] S. Winter, T. Wittchen, J. Metzdorf, in *Proc. 16th European Photovoltaic Solar Energy Conf.*, Routledge, Glasgow **2000**, pp. 2198–2201, ISBN 9781902916187.

[13] W. Warta, J. Hohl-Ebinger, A. Ohm, K. Kordelos, S. Winter, R. Adelhelm, D. Berger, H.-P. Hartmann, D.-H. Neuhaus, M. Wald, T. Kieliba, H. Albert, B. Hund, J. Isenberg, H. Nagel, J. Fölsch, P. Grabitz, W. Lattwein, in *24th European Photovoltaic Solar Energy Conf.*, WIP, München, Germany **2009**, pp. 1382–1386.

[14] K. Bothe, D. Hinken, *Photovolt. Int.* **2019**, *43*, 74.

[15] I. Kröger, D. Friedrich, S. Winter, in *IEEE 7th World Conf. on Photovoltaic Energy Conversion, WCPEC 2018 - A Joint Conf. of 45th IEEE PVSC, 28th PVSEC and 34th EU PVSEC*, IEEE, Piscataway, NJ **2018**, *3*, p. 3492.

[16] S. W. Brown, G. P. Eppeldauer, K. R. Lykke, *Appl. Optics* **2006**, *45*, 8218.

[17] S. Winter, T. Fey, D. Friedrich, I. Kröger, K. Von Volkmann, in *Proc. of the 26th European Photovoltaic Solar Energy Conf. and Exhibition*, WIP, München, Germany **2011**, pp. 3466–3468.

[18] K. Bothe, D. Hinken, B. Min, C. Schinke, *IEEE J. Photovolt.* **2018**, *8*, 611.

[19] S. Tulloch, The Design and Use of LED Reference Light Sources for Q.E. Calibration, Technical report, Instrument Science Group Royal Greenwich Observatory, **1996**.

[20] D. L. Young, B. Egaas, S. Pinegar, P. Stradins, in *33rd IEEE Photovoltaic Specialists Conf.*, IEEE, Piscataway, NJ **2008** pp. 1–3.

[21] B. H. Hamadani, J. Roller, B. Dougherty, H. W. Yoon, in *Conf. Record of the IEEE Photovoltaic Specialists Conf.*, IEEE, Piscataway, NJ 2013, pp. 73–75.

[22] A. Paduthol, M. K. Juhl, T. Trupke, *IEEE J. Photovoltaics* **2018**, *8*, 559.

[23] M. Turek, K. Sporleder, T. Luka, *Sol. Energy Mater. Sol. Cells* **2019**, *194*, 142.

[24] C. Edmonds, H. Mullejans, *IEEE J. Photovoltaics* **2022**, *13*, 133.

[25] D. Hinken, I. Kröger, S. Winter, R. Brendel, K. Bothe, *Metrologia* **2019**, *30*, 1.

[26] W. Press, S. Teukolsky, W. Vetterling, B. Flannery, in *Numerical Recipes 3rd Edition: The Art Of Scientific Computing*, Cambridge University Press, Cambridge, UK **2007**.

[27] I. Bronstein, K. Semendjajew, G. Musiol, H. Mühlig, in *Taschenbuch der Mathematik*, Deutsch, **2001**.

[28] C. Schinke, H. Pollex, D. Hinken, M. Wolf, K. Bothe, I. Kröger, S. Nevas, S. Winter, *Metrologia* **2020**, *57*, 6.

[29] International Standard IEC 60904-09, Edition 3.0, 2020-09, Photovoltaic Devices - Part 9: Classification of Solar Simulator Characteristics.

[30] G. Van Rossum, F. L. Drake, in *Python 3 Reference Manual*, CreateSpace, Scotts Valley, CA **2009**.

[31] P. Virtanen, R. Gommers, T. E. Oliphant, M. Haberland, T. Reddy, D. Cournapeau, E. Burovski, P. Peterson, W. Weckesser, J. Bright, S. J. van der Walt, M. Brett, J. Wilson, K. J. Millman, N. Mayorov, A. R. J. Nelson, E. Jones, R. Kern, E. Larson, C. J. Carey, I. Polat, Y. Feng, E. W. Moore, J. VanderPlas, D. Laxalde, J. Perktold, R. Cimrman, I. Henriksen, E. A. Quintero, C. R. Harris, et al., *Nat. Methods* **2020**, *17*, 261.

[32] C. R. Osterwald, S. Anevsky, K. Bücher, A. K. Barua, P. Chaudhuri, J. Dubard, K. Emery, B. Hansen, D. King, J. Metzdorf, F. Nagamine, R. Shimokawa, Y. X. Wang, T. Wittchen, W. Zaaiman, A. Zastrow, J. Zhang, *Progr. Photovoltaics: Res. Appl.* **1999**, *7*, 287.

[33] Bigref Large Area PV Reference Cell, https://www.imt-solar.com/solar-irradiance-sensors/bigref/, (accessed: March 2023).

[34] JCGM 2008:100, International Organization for Standardization, Geneva **2008**, p. 134.

[35] I. Kröger, D. Friedrich, S. Winter, E. Salis, H. Müllejans, D. Pavanello, J. Hohl-Ebinger, K. Bothe, D. Hinken, S. Dittmann, G. Friesen, M. Bliss, T. Betts, R. Gottschalg, L. Rimmelspacher, J. Stang, W. Herrmann, J. Dubard, *Int. J. Metrol. Qual. Eng.* **2018**, *9*, 8.

[36] D. A. Jacobs, Y. Wu, H. Shen, C. Barugkin, F. J. Beck, T. P. White, K. Weber, K. R. Catchpole, *Phys. Chem. Chem. Phys.* **2017**, *19*, 3094.

[37] M. Bliss, A. Smith, T. R. Betts, J. Baker, F. De Rossi, S. Bai, T. Watson, H. Snaith, R. Gottschalg, *IEEE J. Photovoltaics* **2019**, *9*, 220.